Since January 2020 Elsevier has created a COVID-19 resource centre with free information in English and Mandarin on the novel coronavirus COVID-19. The COVID-19 resource centre is hosted on Elsevier Connect, the company's public news and information website.

Journal of Molecular Liquids 312 (2020) 113454

Contents lists available at ScienceDirect

Journal of Molecular Liquids

journal homepage: www.elsevier.com/locate/molliq

Short Communication

Au-decorated BN nanotube as a breathalyzer for potential medical applications

Chenjiao Ge [a,b], Mingli Li [c,*], Mingxuan Li [d], Ali Ahmadi Peyghan [e,*]

[a] Jilin Jianzhu University of Changchun, Changchun 130118, China
[b] HIT(Hainan) Military-Civilian Integration Innovation Research Institute Co., LTD, Hainan Province 572400, China
[c] Department of Life Science and Engineering, Jining University, Jining 273155, China
[d] Nursing Department, Affiliated Hospital of Jining Medical University, Jining 272000, China
[e] Tarbiat Modares University, Tehran, Iran

ARTICLE INFO

Article history:
Received 9 April 2020
Received in revised form 22 May 2020
Accepted 26 May 2020
Available online 28 May 2020

Keywords:
COVID-19
Biomarker
Sensor
NO gas
Density functional theory

ABSTRACT

Respiratory viral infections such as coronavirus (COVID-19) will cause a great mortality, especially in people who underly lung diseases such as chronic obstructive pulmonary and asthma. Very recently, the COVID-19 outbreak has exposed the lack of quick approaches for screening people who may have risen risk of pathogen contact. One proposed non-invasive potential approach to recognize the viral infection is analysis of exhaled gases. It has been indicated that the nitric oxide is one of most important biomarkers which might be emanated by respiratory epithelial cells. Using density functional theory calculations, here, we introduced a novel Au-decorated BN nanotube-based breathalyzer for probable recognition of NO gas released from the respiratory epithelial cells in the presence of interfering CO_2 and H_2O gases. This breathalyzer benefits from different advantages including high sensitivity (sensing response = 101.5), high selectivity, portability, short recovery time (1.8 μs at 298 K), and low cost.

1. Introduction

Very recently, an outbreak of unexplained pneumonia has been caused by a new coronavirus infection called COVID-19 [1]. Usual symptoms are shortness of breath, cough, and fever [2]. Other symptoms might include sore throat, loss of smell or taste, abdominal pain, sputum production, diarrhea, and muscle pain [2]. While the most of cases result in minor symptoms, some progress to multi-organ failure, severe acute respiratory syndrome, pneumonia, kidney failure, and death [3]. As of May 22, 2020, more than 335,000 deaths were reported in worldwide that the overall death rate per number of diagnosed cases has been predicted to be 4.5%; ranging from 0.2% to 15% depending on the age and other health problems [4]. The COVID-19 outbreak has exposed the lack of quick non-invasive approaches for screening people who may have risen risk of pathogen contact. In contrary to the bacterial infections, in which toxins generated by the infectious agent origin much of the pathology, the symptoms of COVID-19 are due to the host response to the virus. Upon the virus infection, pro-inflammatory cytokines are released that lead to the constellation of lethargy, malaise, diffuse pain, and fatigue in addition to the early fever [5].

A usual feature of the inflammatory response in patients is the volatile organic compounds and nitric oxide (NO) production of the airway epithelium and alveolar and also, from leukocytes that penetrate the lungs [5]. It should be noted that the time course of appearance of these biomarkers nearly coincides with the time course of symptoms of disease. However, detection of these biomarkers in breath can help to recognize the virus infection. Now, different approaches are available and reported [6,7] to detect biomarkers of inflammation in the respiratory system, including specific ion flow tube/mass spectroscopy (SIFT/MS), and gas chromatography/mass spectroscopy (GC/MS). However, these methods are not amenable to be applied without specialized training and cannot be regarded as portable for application in public places or homes where screening of individuals is of great importance. Recently, different nanostructures have been introduced as one of the most promising candidates for developing sensing devices owing to their excellent properties such as high surface/volume ratio, short analysis time, low-temperature action, possibility of miniaturization, low-cost, good sensitivity, and fast response [8–16]. Nanostructure-based sensors are certainly compact enough to be simply deployed. Volatile organic compound based nano-breathalyzers have been formerly introduced and described [17–19]. This manuscript focuses on a novel NO-based nano-breathalyzer to be applied in the COVID-19 virus infection detection.

One-dimensional (1D) nanostructures have attracted considerable attention in manufacturing highly sensitive and portable gas sensors [19]. For 1D nanostructures, the effective adsorption places for gas molecules increase because of the relatively great specific surface area,

* Corresponding authors.
E-mail addresses: lmliml791@163.com (M. Li), ahmadi.iau@gmail.com (A.A. Peyghan).

https://doi.org/10.1016/j.molliq.2020.113454
0167-7322/

which might simplify the surface adsorption process providing large surface charge densities [20]. Numerous 1D nanostructures have been introduced to date to be used in gas sensors, including ZnO, SnO_2, and Al_2O_3 nanowires, and TiO_2, BC_3, BC_2N, and carbon nanotubes [21–24]. Because of the multiplicity and complexity of the environment, it is a universal need to develop gas sensing devices that can be applied in a wild environment. Boron nitride nanotubes (BNNTs) are attractive as 1D nanostructures owing to their superior intrinsic physical and chemical characteristics. They display excellent thermal and mechanical properties, and also have a high resistance to oxidation at high temperatures and great chemical stability [25]. These exceptional characteristics make BNNTs very suitable for several applications, particularly in high-temperature and hazardous environments. However, being a high stable semiconductor, BNNTs have a low tendency to interact with gas molecules [24,26,27] that limits their applications in fabricating breathalyzers. In order to overcome this drawback, several approaches are accessible, including chemical functionalization, creating defects in the structure of nanomaterials, doping or decorating of impurity atoms. Recently, Yu et al. have synthesized Au-decorated BNNTs (Au@BNNTs), indicating that the reactivity and sensitivity of the BNNTs significantly changed by the Au-decoration [28]. The successful synthesis of Au@BNNTs suggests a low-cost and simple method for detecting different gas molecules.

However, it is an interesting issue that to discover how the Au atoms can influence the sensitivity of BNNTs toward the gas molecules. Density functional theory (DFT) is a powerful method which can be applied to inspect such matters, explaining the experimental observations at molecular level. Here, we performed a DFT study to investigate the probable application of pristine BNNTs and Au@BNNTs as breathalyzer to sense the exhaled NO gas in the presence of CO_2 and H_2O gases for diagnosis of COVID-19. We present a new computational method to explore the effect of Au-decoration on the sensitivity of BNNTs according to the experimental reports.

2. Computational methods

All of the calculations were carried out by the software of GAMESS [29]. It has been previously specified that meta-generalized gradient approximation TPSS functional predicts the most accurate and reliable results for molecular properties of transition metal containing structures [30]. Also, they recommended the LANL2DZ (on the transition metal) + 6–31+G** mixed basis set. Accordingly, herein, the structure optimizations and natural bond orbitals (NBO), electronic, energetic, and charge analyses were performed applying the TPSS functional with the LANL2DZ basis set on the Au atoms and 6–31 + G** on the others. The dispersion interaction evaluation is the drawback of the standard DFT functionals. Therefore, the TPSS functional was augmented with a Grimme D3 term to predict the dispersion forces [31]. For the calculation of adsorption energies (E_{ad}) of an adsorbate on the surface of an adsorbent, the following equation was employed:

$$E_{ad} = E(\text{complex}) - E(\text{adsorbate}) - E(\text{adsorbent}) + E_{BSSE} \quad (1)$$

Adsorbate may be an Au atom, O_2 or NO molecule. The adsorbent may be a pristine BNNT, Au@BNNT, or O_2 adsorbed Au@BNNT (O_2/Au@BNNT). The E_{BSSE} designates the basis set superposition error computed by the counterpoise method [32]. The transition state structure was predicted using the synchronous transit-guided quasi-Newton (STQN) technique [33].

3. Results and discussion

3.1. The pristine BNNT

We selected a (12,0) *zigzag* single-walled BNNT ($B_{108}N_{108}H_{24}$) as shown in Fig. 1. The predicted length and diameter of the optimized

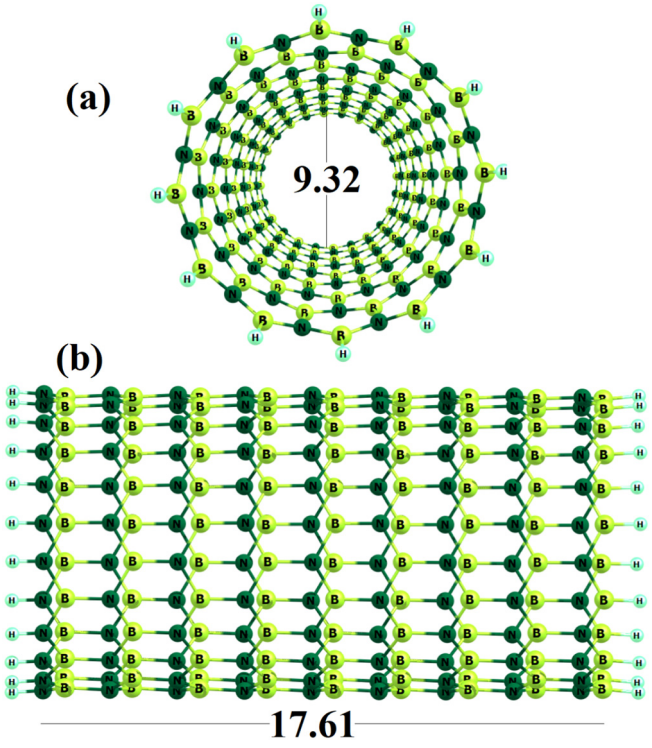

Fig. 1. The side and top views of optimized geometry of BNNT. Distances are in Å.

tube are about 17.61 and 9.32 Å, respectively. Two kinds of B—N bonds were recognized being parallel or diagonal to the tube axis with length of 1.45 or 1.47 Å. The HOMO and LUMO energies of the BNNT are −5.463 and −1.451 eV (Table 1), respectively, creating an E_g about 4.012 eV. As mentioned before, experimental works have indicated that the working mechanism of gas sensors depends on the change of the sensor resistivity (or conductivity) because of the charge transfer between the gas molecules and sensors [19]. The sensing mechanism is based on the fact that initially the O_2 molecules of the atmosphere adsorb on the sensor surface, extracting some electrons from the conduction band to yield the O anion species O^-, O^{2-}, or O_2^-, changing the electrical conductance of the sensor. Then, if a reducing gas like NO reacts with the O ions on the sensor surface, the ions give some of the trapped electrons back into the sensor material. Consequently, the electrical conductance somewhat backs to the initial value. Here, all reactions which should be occurred on the surface of BNNT for the NO sensing are summarized as follows:

$$O_{2(gas)} \text{ of air} \rightarrow O_{2(ads)} \quad (3)$$

$$O_{2(ads)} + 2e^- \rightarrow 2O^-_{(ads)} \quad (4)$$

$$2NO_{(ads)} + 2O^-_{(ads)} \rightarrow 2NO_2 + 2e^- \quad (5)$$

Previous works have shown that the pristine BNNTs weakly adsorb the O_2 gas and the reactions of Eqs. (4) and (5) cannot be occurred

Table 1
Adsorption energy (E_{ad}, kcal/mol) for Au atom on the pristine BNNT (Fig. 2). Energy of Fermi level (E_F), HOMO, and LUMO, and HOMO-LUMO energy gap (E_g) in eV.

Structure	E_{ad}	E_{HOMO}	E_F	E_{LUMO}	E_g
BNNT	–	−5.463	−3.457	−1.451	4.012
I	−31.7	−5.154	−4.092	−3.029	2.125
II	−28.1	−5.233	−4.118	−3.003	2.230
III	−20.5	−5.256	−4.131	−3.005	2.251

[34–36]. Thus, the pristine BNNT cannot detect the NO gas. To overcome this problem, we suggested the Au-decoration into the surface of BNNT.

3.2. Au@BNNT

To obtain the most stable Au@BNNT geometry, we tested some starting configurations by adding an Au atom on different sites of the BNNT, including on the B or N atom, above bridge sites of B—N bonds, and above the center of a B_3N_3 hexagonal ring. Full structural optimization was then performed with each initial complex. It was found that the most stable Au@BNNT is that in which the Au atom adsorbed above the hollow site of the B_3N_3 hexagon ring with Au…B interaction distances of 2.71 and 2.80 Å as shown in Fig. 1 (complex **I**). The E_{ad} for Au adsorption on the BNNT is −31.7 kcal/mol in the complex **I**, signifying an exothermic and favorable process. The Au-decoration meaningfully reduced the E_g value of BNNT from 4.012 to 2.125 eV because of a large stabilization in the LUMO level. Also, two other local minima are predicted which are labeled by **II** and **III** as shown in Fig. 2. In the complex **II**, the Au atom located on a B atom at a distance of 2.34 Å with E_{ad} of −28.1 kcal/mol. In the complex **III**, the Au atom located on an N atom at a distance of 2.39 Å with E_{ad} of −20.5 kcal/mol. The results indicate that as the Au is a metal, it tends to interact with the electron deficient sites (B atoms) compared to the electron rich sites (N atoms).

We selected the most stable Au@BNNT structure (**I**) and then studied the adsorption of an O_2 molecule on its surface as the first step (Eq. (3)) for detection of NO gas of exhaled breath. Fig. 3 indicates that an O_2 molecule powerfully adsorbed on the Au atom with an E_{ad} of −25.2 kcal/mol (Table 2), and the O—Au interaction distance of 2.10 Å. After the O_2 adsorption, the O—O bond length elongated from 1.23 to 1.33 Å, weakening this bond. It indicates that the Au metal catalyzes the dissociation of O_2 gas and facilitates the oxygen ion formation on the surface of the Au@BNNT. Based on the frontier molecular orbital analysis, the LUMO level (Fig. 2) is mainly restricted on the surface of Au atom in the Au@BNNT (**I**) which makes it a promising site for O_2 adsorption. It should be noted that the O—O bond length of the free O_2^- molecule is calculated to be 1.36 Å. In the free O_2^- molecule an electron is inserted to the π_{2p}^* orbital and the spin multiplicity is doublet. Based on the NBO analysis, the O_2 molecule extracts 0.86 |e| from the surface of Au@BNNT. Consequently, it can be deduced that the Au-decoration on the BNNT considerably increases the conversion of O_2 to O anions.

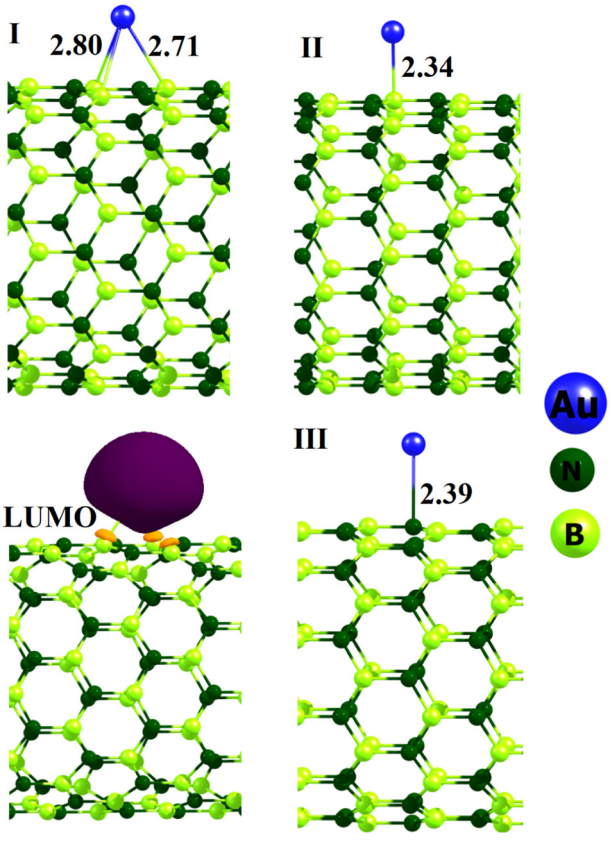

Fig. 2. Optimized structures of Au-decorated BNNT and the LUMO profile of complex **I**. Distance is in Å.

The results of Table 2 show that the electronic properties of Au@BNNT were meaningfully perturbed by the O_2 molecule interaction. Its LUMO level intensely stabilizes by shifting from −3.029 to −3.214 eV and the HOMO energy is slightly changed. Therefore, the E_g of Au@BNNT dramatically decreased from 2.125 to 1.936 eV, which will increase the electrical conductance of the Au@BNNT according to the Eq. (6):

$$\sigma = AT^{3/2}\ \exp(-E_g/2kT) \tag{6}$$

where A is a constant in dimension of electrons/$m^3K^{3/2}$ and k the Boltzmann's constant. This equation states that a reduction in the E_g exponentially increases the electrical conductance of adsorbent, linking to the gas presence. Additionally, the Fermi level of Au@BNNT moves from −4.092 to −4.182 eV. This shows that the electron emission will decrease from the surface of Au@BNNT by the O_2 adsorption.

Next, we explored the adsorption of breath exhaled NO gas on the pre-adsorbed O_2 molecule as shown in Fig. 4. The $(NO)_2/O_2$/Au@BNNT complex displays that upon the adsorption of two NO molecules, they react with the pre-chemisorbed O ions and yield two NO_2 molecules. This reaction releases some of the trapped electrons by O anions back into the Au@BNNT. The remaining charge on each NO_2 molecules is about 0.15 |e|. The NO_2 molecules then weakly adsorb on the surface of the Au@BNNT (Fig. 4) with E_{ad} of −11.3 kcal/mol per molecule. The NO adsorption on the O_2/Au@BNNT complex has to pass through a transition state structure as exposed in Fig. 4. In the transition state structure, the O—O bonds is weakening by stretching from 1.33 and to 1.55 Å and two new N—O bonds are forming with length about 1.40 Å. Our predicted energy barrier is about 5.2 kcal/mol, representing that this process could be occurred at room temperature. After the NO adsorption and generation of NO_2 molecules under catalytic effect of Au atom, the E_g of Au@BNNT somewhat back toward its initial value (by about 0.119 eV, Table 2) due to an electron back-donation process from the O ions to the Au@BNNT.

The E_g may be an electronic parameter to quantity an adsorbent sensitivity toward a gas regarding the relationship between the electrical conductance and E_g based on the Eq. (6). The sensor response (S) can be obtained from the following equation according to the experimental works:

$$S = |\ R_2 - R_1\ |\ /R_1 = |\ (R_2/R_1) - 1\ | \tag{7}$$

where R_1 and R_2 are the electrical resistance of the Au@BNNT before and after the gas adsorption, respectively. Electrical conductance and resistance are inversely related to each other. Thus, we one can write:

$$S = |\ (\sigma_1/\sigma_2) - 1\ | = \exp(|\Delta E_g|/kT) - 1 \tag{8}$$

where ΔE_g is the E_g change after the gas adsorption on the adsorbent. Using Eq. (8), the response of Au@BNNT to NO gas is 101.5 at 298 K, demonstrating that the Au@BNNT is highly sensitive to NO gas. This indicates that the Au@BNNT may be applied as a breathalyzer for diagnosis of COVID-19.

3.3. Recovery time

The strength of an interaction is a critical parameter for sensor growth for because a strong interaction, the desorption process

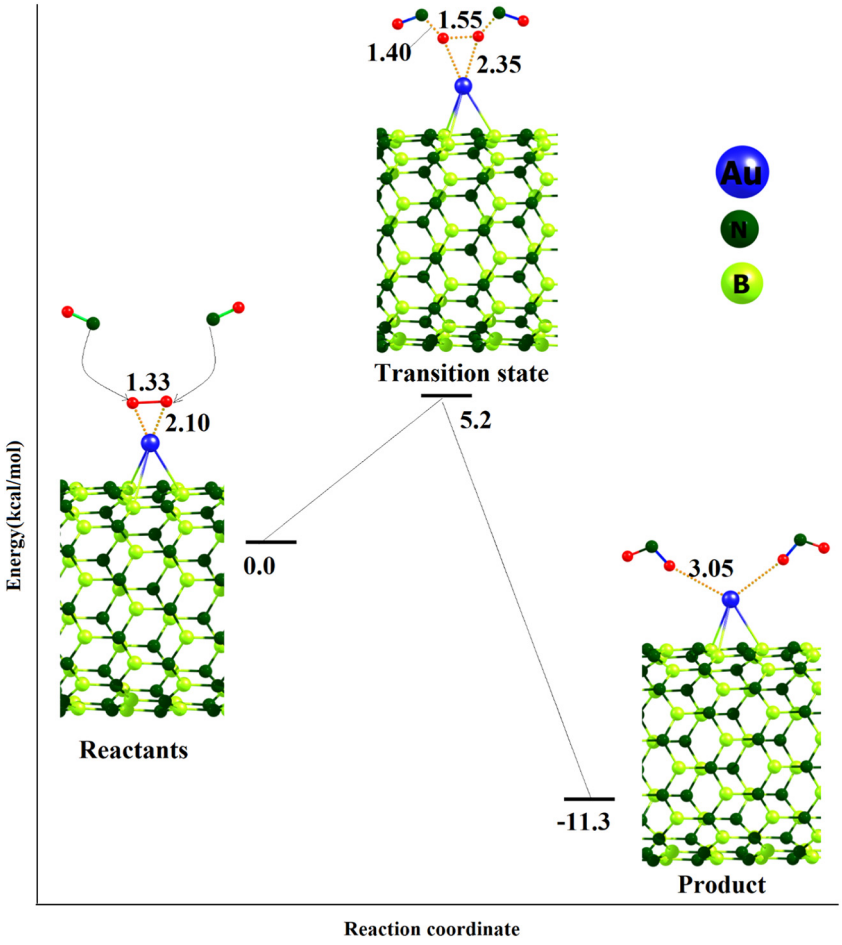

Fig. 3. A schematic diagram for NO adsorption on the pre-oxygen adsorbed Au@BNNT to produce NO_2 gas. Distances are in Å.

becomes hard. A shorter recovery time will be gotten with a smaller desorption energy (E_{des}) based on the following equation:

$$\tau = \upsilon_0^{-1} \exp(-E_{des}/kT) \quad (9)$$

where ν_0, T, and k are the attempt frequency, the temperature, the Boltzmann's constant (~2.0×10^{-3} kcal/mol·K), respectively. In fact, Eq. (9) is the transition state theory. Although it has been applied to rate processes for gas phase reactions, there exist numerous examples in which this equation has been applied to gas desorption from solid surfaces [37–39]. On the other hand, experimentally, for gas desorption, thermal energy or irradiation of different photonic frequencies (υ_0) can be used [40,41]. Here, for recovery time calculation, first, we should calculate the average E_{des} per molecule for desorption of the produced NO_2 molecules from the surface of Au@BNNT. To this aim, we employed the following equation:

$$E_{des} = [E(Au@BNNT) + 2\,E(NO_2) - E(complex) - E_{BSSE}]/2 \quad (10)$$

Table 2
Adsorption energy (E_{ad}, kcal/mol) for O_2 and NO adsorption on the BNNT and O_2/BNNT, respectively. Energy of Fermi level (E_F), HOMO, and LUMO, and HOMO-LUMO energy gap (E_g) in eV. The ΔE_g indicates the change of E_g after the adsorption process. Q is the average charge on the adsorbates on the BNNT.

Structure	E_{ad}	E_{HOMO}	E_F	E_{LUMO}	E_g	ΔE_g	Q(e)
Au@BNNT	–	−5.154	−4.092	−3.029	2.125	–	–
O_2/Au@BNNT	−25.2	−5.150	−4.182	−3.214	1.936	−0.189	−0.86
NO/O_2/Au@BNNT	−11.3	−5.152	−4.125	−3.097	2.055	0.119	−0.30

where E(Au@BNNT) and E(NO_2) are energies of a single Au@BNNT and NO_2, respectively. E(complex) is the energy of the final complex in which two NO_2 molecules are adsorbed on the surface of an Au@BNNT (Fig. 3). However, the E_{des} was calculated to be 9.9 kcal/mol. Therefore, the recovery time is predicted to be 1.8 μs at 298 K and the ultra-violet light ($\upsilon \sim 10^{13}\ s^{-1}$), indicating a short time for sensor recovery.

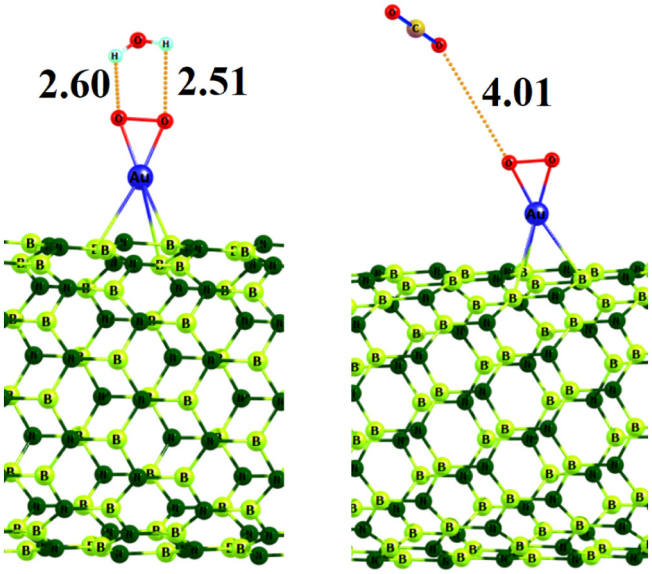

Fig. 4. Optimizes structures of H_2O/O_2/Au@BNNT and CO_2/O_2/Au@BNNT. Distances are in Å.

3.4. Selectivity

Finally, in order to further investigate the selectivity of Au@BNNT toward different gas molecules, we explored the interaction of two CO_2 and H_2O gases with the O_2/Au@BNNT because they are the most abundant gases in the exhaled breath. Our results designate that the nonpolar CO_2 gas weakly interacts with the pre-adsorbed O_2 on the Au@BNNT (Fig. 4) with E_{ad} of −0.9 kcal/mol and no charge transfer. The E_g value of O_2/Au@BNNT decreased from 2.125 to 2.121 eV upon the CO_2 adsorption. It indicates that the effect of the nonpolar gas molecules on the electronic properties of O_2/Au@BNNT is negligible. However, the polar H_2O gas somewhat strongly interacts with the O_2/Au@BNNT compared to the nonpolar CO_2 molecules with E_{ad} of −2.7 kcal/mol because of forming a hydrogen bonding with distance of 3.2 Å. The E_g value of O_2/Au@BNNT increased by about 0.029 eV upon the adsorption of H_2O gas because of a charge transfer about 0.06 |e| from O_2/Au@BNNT to the H_2O molecule. Thus, the sensing response of O_2/Au@BNNT is about 2.1 which is negligible compared to its response toward NO gas (~101.5). Consequently, we deduced that the Au@BNNT could sense the exhaled NO gas in the presence of H_2O, and CO_2 gases.

4. Conclusions

Very recently, new respiratory viral infection COVID-19 caused a great mortality. Thus, finding fast and portable sensors for screening people who may have risen risk of pathogen contact is of great importance. One proposed potential approach to recognize the viral infection is analysis of exhaled gases. It has been indicated that the nitric oxide is one of most important biomarkers which might be emanated by respiratory epithelial cells. Here, DFT calculations were applied to investigate the probable application of Au@BNNT as a breathalyzer to detect exhaled NO gas as a symptom of COVID-19 infection. It was found that by the Au-decoration on the surface of BNNT, the O_2 molecules of air adsorb on the Au atom, weakening the O—O bond which makes it favorable site for NO attack and NO_2 formation. This process required a small energy barrier of 5.2 kcal/mol which makes it possible at room temperature. We predicted a short recovery time and high sensing response of 1.8 μs and 101.5 at 298 K for Au@BNNT as an NO sensor. The results indicate that the Au@BNNT is a promising breathalyzer to be applied in the exhaled NO gas sensors.

CRediT authorship contribution statement

Chenjiao Ge: Data curation, Conceptualization. **Mingli Li:** Methodology, Software, Supervision, Writing - review & editing. **Mingxuan Li:** Funding acquisition, Project administration. **Ali Ahmadi Peyghan:** Writing - original draft, Supervision, Investigation.

Declaration of competing interest

The authors declare that they have no known competing financial interests or personal relationships that could have appeared to influence the work reported in this paper.

Acknowledgements

The study was supported by “Science and Technology Project of China Railway Corporation, China (Grant No. 1341324011)”.

References

[1] M.N.K. Boulos, E.M. Geraghty, Geographical tracking and mapping of coronavirus disease COVID-19/severe acute respiratory syndrome coronavirus 2 (SARS-CoV-2) epidemic and associated events around the world: how 21st century GIS technologies are supporting the global fight against outbreaks and epidemics, BioMed Central 19 (2020) 8–19.
[2] C.P.E.R.E. Novel, The epidemiological characteristics of an outbreak of 2019 novel coronavirus diseases (COVID-19) in China, Zhonghua liu xing bing xue za zhi= Zhonghua liuxingbingxue zazhi 41 (2020) 145.
[3] Z. Xu, L. Shi, Y. Wang, J. Zhang, L. Huang, C. Zhang, S. Liu, P. Zhao, H. Liu, L. Zhu, Pathological findings of COVID-19 associated with acute respiratory distress syndrome, Lancet Respir. Med. 8 (2020) 420–422.
[4] https://www.worldometers.info/coronavirus/coronavirus-death-rate/.
[5] P.-I. Gouma, L. Wang, S.R. Simon, M. Stanacevic, Novel isoprene sensor for a flu virus breath monitor, Sensors 17 (2017) 199.
[6] A. Mashir, K.M. Paschke, D. van Duin, N.K. Shrestha, D. Laskowski, M.K. Storer, B. Yen-Lieberman, S.M. Gordon, M. Aytekin, R.A. Dweik, Effect of the influenza A (H1N1) live attenuated intranasal vaccine on nitric oxide (FE NO) and other volatiles in exhaled breath, Journal of Breath Research 5 (2011), 037107.
[7] M. Phillips, R.N. Cataneo, A. Chaturvedi, P.J. Danaher, A. Devadiga, D.A. Legendre, K.L. Nail, P. Schmitt, J. Wai, Effect of influenza vaccination on oxidative stress products in breath, Journal of Breath Research 4 (2010), 026001.
[8] M. Kamel, A. Morsali, H. Raissi, K. Mohammadifard, Theoretical insights into the intermolecular and mechanisms of covalent interaction of Flutamide drug with COOH and COCl functionalized carbon nanotubes: a DFT approach, Chemical Review and Letters 3 (2020) 23–37.
[9] R. Dos Santos, R. Rivelino, F. de Brito Mota, G. Gueorguiev, A. Kakanakova-Georgieva, Dopant species with Al–Si and N–Si bonding in the MOCVD of AlN implementing trimethylaluminum, ammonia and silane, J. Phys. D. Appl. Phys. 48 (2015), 295104.
[10] R. Rostamoghli, M. Vakili, A. Banaei, E. Pourbashir, K. Jalalierad, Applying the B12N12 nanoparticle as the CO, CO2, H2O and NH3 sensor, Chemical Review and Letters 1 (2018) 31–36.
[11] J. Beheshtian, A.A. Peyghan, M.B. Tabar, Z. Bagheri, DFT study on the functionalization of a BN nanotube with sulfamide, Appl. Surf. Sci. 266 (2013) 182–187.
[12] H. Ghafur Rauf, S. Majedi, E. Abdulkareem Mahmood, M. Sofi, Adsorption behavior of the Al-and Ga-doped B12N12 nanocages on COn (n= 1, 2) and HnX (n= 2, 3 and X= O, N): a comparative study, Chemical Review and Letters 2 (2019) 140–150.
[13] R. Freitas, G.K. Gueorguiev, F. de Brito Mota, C. De Castilho, S. Stafström, A. Kakanakova-Georgieva, Reactivity of adducts relevant to the deposition of hexagonal BN from first-principles calculations, Chem. Phys. Lett. 583 (2013) 119–124.
[14] E. Babanezhad, A. Beheshti, The possibility of selective sensing of the straight-chain alcohols (including methanol to n-pentanol) using the C20 fullerene and C18NB nano cage, Chemical Review and Letters 1 (2018) 82–88.
[15] F. Li, H. Asadi, DFT study of the effect of platinum on the H2 gas sensing performance of ZnO nanotube: explaining the experimental observations, J. Mol. Liq. 309 (2020), 113139.
[16] S.A. Siadati, S. Rezazadeh, Switching behavior of an actuator containing germanium, silicon-decorated and normal C20 fullerene, Chemical Review and Letters 1 (2018) 77–81.
[17] P. Gouma, A. Prasad, S. Stanacevic, A selective nanosensor device for exhaled breath analysis, Journal of Breath Research 5 (2011), 037110.
[18] P.I. Gouma, A.K. Prasad, K.K. Iyer, Selective nanoprobes for ‘signalling gases’, Nanotechnology 17 (2006) S48–S53.
[19] J. Huang, Q. Wan, Gas sensors based on semiconducting metal oxide one-dimensional nanostructures, Sensors 9 (2009) 9903–9924.
[20] J. Weber, R. Singhal, S. Zekri, A. Kumar, One-dimensional nanostructures: fabrication, characterisation and applications, Int. Mater. Rev. 53 (2008) 235–255.
[21] F. Torrens, G. Castellano, Nanostructures cluster models in solution: Extension to C, BC2N, and BN fullerenes, tubes, and cones, Contemporary Advancements in Information Technology Development in Dynamic Environments, IGI Global 2014, pp. 221–253.
[22] H. Tang, K. Prasad, R. Sanjines, F. Levy, TiO2 anatase thin films as gas sensors, Sensors Actuators B Chem. 26 (1995) 71–75.
[23] B.M. Venkatesan, A.B. Shah, J.M. Zuo, R. Bashir, DNA sensing using nanocrystalline surface-enhanced Al2O3 nanopore sensors, Adv. Funct. Mater. 20 (2010) 1266–1275.
[24] T.-J. Hsueh, C.-L. Hsu, S.-J. Chang, I.-C. Chen, Laterally grown ZnO nanowire ethanol gas sensors, Sensors Actuators B Chem. 126 (2007) 473–477.
[25] D. Golberg, Y. Bando, C. Tang, C. Zhi, Boron nitride nanotubes, Adv. Mater. 19 (2007) 2413–2432.
[26] M. Terrones, J. Romo-Herrera, E. Cruz-Silva, F. López-Urías, E. Munoz-Sandoval, J. Velázquez-Salazar, H. Terrones, Y. Bando, D. Golberg, Pure and doped boron nitride nanotubes, Mater. Today 10 (2007) 30–38.
[27] J. Beheshtian, A.A. Peyghan, Z. Bagheri, Detection of phosgene by Sc-doped BN nanotubes: a DFT study, Sens. Actuators B: Chem. (2012) 846–852.
[28] Y. Yu, H. Chen, Y. Liu, L.H. Li, Y. Chen, Humidity sensing properties of single au-decorated boron nitride nanotubes, Electrochem. Commun. 30 (2013) 29–33.
[29] M.W. Schmidt, K.K. Baldridge, J.A. Boatz, S.T. Elbert, M.S. Gordon, J.H. Jensen, S. Koseki, N. Matsunaga, K.A. Nguyen, S. Su, T.L. Windus, M. Dupuis, J.A. Montgomery, J. Comp. Chem. 14 (1993) 1347–1363.
[30] Y. Yang, M.N. Weaver, K.M. Merz, Assessment of the “6-31+G** + LANL2DZ” mixed basis set coupled with density functional theory methods and the effective Core potential: prediction of heats of formation and ionization potentials for first-row-transition-metal complexes, J. Phys. Chem. A 113 (2009) 9843–9851.
[31] S. Grimme, Accurate description of van der Waals complexes by density functional theory including empirical corrections, J. Comput. Chem. 25 (2004) 1463–1473.
[32] S.F. Boys, F. Bernardi, The calculation of small molecular interactions by the differences of separate total energies. Some procedures with reduced errors, Mol. Phys. 19 (1970) 553–566.
[33] C. Peng, H. Bernhard Schlegel, Combining synchronous transit and quasi-newton methods to find transition states, Israel Journal of Chemistry 33 (1993) 449–454.

[34] Y. Chen, C.-L. Hu, J.-Q. Li, G.-X. Jia, Y.-F. Zhang, Theoretical study of O2 adsorption and reactivity on single-walled boron nitride nanotubes, Chem. Phys. Lett. 449 (2007) 149–154.
[35] J. Zhang, K.P. Loh, J. Zheng, M.B. Sullivan, P. Wu, Adsorption of molecular oxygen on the walls of pristine and carbon-doped (5, 5) boron nitride nanotubes: spin-polarized density functional study, Phys. Rev. B 75 (2007), 245301.
[36] R. Geetha, V. Gayathri, Comparative study on gas adsorption in defected carbon and boron nitride nanotube, Curr. Nanosci. 6 (2010) 131–136.
[37] A. Redondo, Y. Zeiri, J.J. Low, W.A. Goddard, Application of transition state theory to desorption from solid surfaces: Ammonia on Ni(111), J. Chem. Phys. 79 (1983) 6410–6415.
[38] The application of transition state theory to gas–surface reactions in Langmuir systems, J. Chem. Phys. 102 (8) (1995) 22 February.
[39] Density functional theory calculations on interface structures and adsorption properties of graphenes: a review, The Open Nanoscience Journal 3 (2009) 34–55.
[40] R. Kumar, N. Goel, M. Kumar, UV-activated MoS2 based fast and reversible NO2 sensor at room temperature, ACS sensors 2 (2017) 1744–1752.
[41] A. Bano, J. Krishna, D.K. Pandey, N. Gaur, An ab initio study of sensing applications of MoB 2 monolayer: a potential gas sensor, Phys. Chem. Chem. Phys. 21 (2019) 4633–4640.